

Curcumin modified Titanium Dioxide Nanotubes with Enhanced Visible Light Photocatalytic Performance

Montri Aiempnanakit¹, Thanatchaporn Tabtimsri², Narit Triamnak³, Cheewita Suwanchawalit^{2}*

¹ Department of Physics, Faculty of Science, Silpakorn University, Sanam Chandra Palace Campus, Nakhon Pathom, Thailand 73000

² Department of Chemistry, Faculty of Science, Silpakorn University, Sanam Chandra Palace Campus, Nakhon Pathom, Thailand 73000

³ Department of Materials Science and Engineering, Faculty of Engineering and Industrial Technology, Silpakorn University, Sanam Chandra Palace Campus, Nakhon Pathom, Thailand 73000

*E-mail: suwanchawalit_c@su.ac.th

Received: 10 October 2018 / *Accepted:* 20 November 2018 / *Published:* 5 January 2019

In this study, curcumin modified TiO₂ nanotubes (Cur-TNT) were prepared by a modified impregnation-electrochemical anodization method with 0.01, 0.025, 0.05 mM of curcumin concentrations. The physical properties of the Cur-TNT were studied by several techniques such as X-ray powder diffraction (XRD), scanning electron microscopy (SEM), energy dispersive X-ray spectroscopy (EDS), Fourier-transformed infrared spectroscopy (FT-IR), and UV-Vis diffused reflectance spectroscopy (DRS). The XRD patterns data revealed anatase phase for both the TNT sample and the Cur-TNT samples. The high magnification images from SEM technique showed that the TNT sample and the Cur-TNT samples possess nanotube-like structures with an average diameter of 85 nm. The FT-IR spectra exhibited the characteristic bands of the TiO₂ and hydroxyl groups on the TNT surface. Instead of hydroxyl groups, the characteristic bands of curcumin were observed on the surface of the Cur-TNT samples. The EDS results complementarily confirmed the existence of Ti, O, C as the main elements of the Cur-TNT samples. Interestingly, the DRS spectra of the Cur-TNT samples extended into the visible region. The photocatalytic properties of the Cur-TNT samples were evaluated from the degradation of methylene blue under visible light irradiation. It was found that the Cur-TNT samples exhibited higher photocatalytic performance than the TNT sample. A possible photocatalytic mechanism has also been proposed.

Keywords: TiO₂ nanotubes, Curcumin modified TiO₂, Electrochemical anodization method, Visible photocatalyst, Degradation of methylene blue

1. INTRODUCTION

Removal of organic pollutants from water has always been a challenging issue, therefore, advanced oxidation processes have been explored for their ability to fully mineralize organic pollutants

[1, 2]. In this regard, titanium dioxide (TiO_2) is widely used as a photocatalyst in the processes. Even though, TiO_2 exhibits an excellent photocatalytic activity under UV illumination, it shows low photocatalytic efficiency in the visible light range. This is due to its high band gap energy (3.0–3.2 eV) leading to electron activation with high energy photon such as ultra-violet (UV) light. [3, 4]. Furthermore, TiO_2 shows a high recombination rate between electrons (e^-) and holes (h^+) pairs, hence, it might not be suitable for some photocatalytic applications. To enhance the photocatalytic efficiency, one option is to shift the light absorption toward visible light and extend the lifetime of the photogenerated electron-hole pairs [5, 6]. To overcome these problems, different strategies have been used to modify the TiO_2 surface including metal deposition [6, 7], transition dopings [8-11], non-metal dopings [12-15], dye-sensitized TiO_2 [16-19], and coupling with other narrow-band gap semiconductors [20-22]. Among those methods, dye-sensitized TiO_2 is considered to be an efficient method to modify the photo-response property of TiO_2 particles. This includes some common dye sensitizers such as porphyrin [16], ruthenium dye [17] phthalocyanine [18], and natural dyes [19, 23]. Generally, the dyes adsorbed on the surface of TiO_2 can be excited by visible light. Then, the photo-induced electrons from the dyes are injected into the conduction band of TiO_2 with subsequent formation of $\bullet\text{O}_2^-$ and $\bullet\text{OH}$ with O_2 adsorbed on the TiO_2 surface, leading to the oxidation of organic molecules. Moreover, a high surface area is needed to guarantee a high dye loading. Therefore, TiO_2 nanotubes have received much attention due to their various functional properties and potential applications. Several processing methods have been used to prepare TiO_2 nanotubes, including hydrothermal synthesis [24], anodic aluminium oxide template synthesis [25], and electrochemical anodization [26-28]. As an effective formation method of TiO_2 nanotubes, the anodization process is useful because of low cost and simple fabrication.

In the present work, the TiO_2 nanotubes (TNT) were fabricated by using the electrochemical anodization method. To find the optimized anodization parameters, the effect of NH_4F concentrations on nanotube growth in the ethylene glycol electrolyte system was investigated. The photocatalytic efficiency in the visible light region was improved by using a curcumin modified TiO_2 nanotubes (Cur-TNT) via the impregnation method. The effect of curcumin concentration loaded on the TiO_2 nanotube surface with respect to the crystalline phase, optical properties, and photocatalytic activity were investigated. The synthesized TNT sample and Cur-TNT samples were characterized by various physical techniques such as X-ray diffraction spectrometry (XRD), scanning electron microscopy (SEM), energy dispersive X-ray spectroscopy (EDS), Fourier-transformed infrared spectroscopy (FT-IR), and UV-Vis diffused reflectance spectroscopy (DRS). The photocatalytic activity of the as-prepared Cur-TNT samples was tested using methylene blue (MB) as a model pollutant and compared with pure TNT sample. The generated hydroxyl radical ($\bullet\text{OH}$) during the photocatalytic experiment was investigated. A possible photocatalytic mechanism has been proposed.

2. EXPERIMENTAL

2.1 Materials

Ethylene glycol ($\text{C}_2\text{H}_6\text{O}_2$, Fisher), deionized water (from Barnstead EASYpure II, USA), and ammonium fluoride (NH_4F , Merck) were used to prepare electrolytes for the anodization experiment.

All chemicals were of analytical grade and used as received. All experiments were conducted under room temperature.

2.2 Preparation of initial Ti films

Titanium (Ti) films were deposited in the high power impulse magnetron sputtering (HiPIMS) mode. The deposition process was performed in a high vacuum stainless-steel chamber with a base pressure below 6×10^{-5} mbar using a diffusion pump. Disk 75 mm in diameter and 6 mm thick made of Ti (99.995% purity) was used as sputtering target. The glass substrates (1.5×2.5 cm²) were cleaned ultrasonically in acetone and methanol. The distance between target and substrate was set at 60 mm. Ar (99.9997% purity) flow of 18 sccm was used to provide a sputtering pressure of 8×10^{-3} mbar. For HiPIMS, unipolar pulses with a constant length (t_{on}) of 100 μ s and a frequency of 500 Hz were used. The pulsing unit (home-built supply) was set at the constant power mode with the averaged power of 200 W. The current, voltage and instantaneous power waveforms were monitored in a Keysight Technologies 4000 X-Series Oscilloscopes. All Ti coatings were deposited without intentional heating for a constant deposition time of 2 h with the film thickness of 1300 nm. These Ti Films were used as the anode for the anodization process.

2.3 Preparation of TiO₂ nanotubes (TNT)

TiO₂ nanotubes (TNT) were prepared by using the electrochemical anodization method. Ti films deposited on glass slide were used as initial Ti films. The ethylene glycol electrolyte system was used to control the chemical dissolution of the formed TiO₂ nanotubes. An electrolyte solution of ethylene glycol with ammonium fluoride (NH₄F) and 2 wt% deionized water for nanostructure TiO₂ was used in the film fabrication. The effect of NH₄F concentrations on the microstructure of the obtained TiO₂ films was investigated. The Ti film was used as the anode and platinum (Pt) as the cathode. The distance between the two electrodes was kept at 1.00 cm as shown in Figure 1. Anodization was performed at 60 V for 35 min operating time using a power supply (M10-QS1001 MCP lab electronics, China). After anodization, the as-prepared TiO₂ nanotubes were rinsed in DI water and dried in N₂ gas. The as-prepared TiO₂ nanotubes were calcined at 400 °C for 3 h to improve the anatase crystalline structure of the TiO₂.

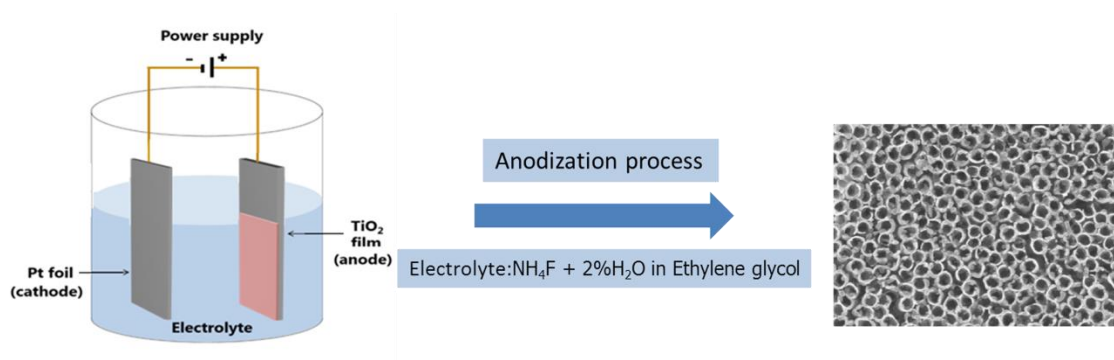


Figure 1. Synthetic route of Titanium dioxide nanotube (TNT) via the anodization process.

2.4 Preparation of Curcumin modified TiO₂ nanotubes (Cur-TNT)

Briefly, the Cur-TNT film was synthesized via the impregnation method. Four nanotube TiO₂ films were immersed in 50 mL curcumin solution with different concentrations of 0.010 mM, 0.025 mM, 0.050 mM for 15 h. After the impregnation process, the Cur-TNT films were washed with ethanol and dried at 80 °C for 12 h. The Cur-TNT films prepared using curcumin concentrations of 0.010 mM, 0.025 mM and 0.050 mM were denoted as 0.01Cur-TNT, 0.025Cur-TNT, and 0.05Cur-TNT, respectively.

2.5 Characterizations

The crystal structure of the as-prepared TNT and Cur-TNT films were determined by X-ray diffraction (XRD) technique recorded by a Rigaku MiniFlex II X-Ray diffractometer with Cu K α radiation (1.5406 Å) from 20° to 80° (2 θ). The morphologies and chemical compositions were investigated by using a scanning electron microscopy (SEM, TESCAN model MIRA3 and FE-SEM, JSM-7001F). Fourier-transformed infrared (FT-IR) spectra were measured by a Perkin Elmer Spectrum Bx spectrophotometer in the range of 400-4000 cm⁻¹ using the attenuated total reflectance (ATR) technique. Optical absorption property and band gap energy were determined using a Shimadzu UV-2401 spectrophotometer.

2.6 Photocatalytic experiment

The photocatalytic performances of the as-prepared TiO₂ nanotubes films were evaluated by the photocatalytic degradation of methylene blue under visible light using an 18W fluorescence lamp as a visible light source [6, 29, 30]. Briefly, four pieces of as-prepared TiO₂ nanotubes films were immersed in 50 mL methylene blue solution (MB, 1.0×10⁻⁵M) in the dark for 1 h and then irradiated under a fluorescence lamp for the pre-determined time. After pre-determined time intervals, the MB solution was collected and the residue concentration of MB was measured at 664 nm with a UV-Vis spectrophotometer (Agilent HP model 8453).

The photocatalytic efficiency of the as-prepared TiO₂ nanotubes films was measured in terms of the degradation efficiency (%) by the following equation:

$$\text{The photocatalytic efficiency (\%)} = \frac{A_0 - A_i}{A_0} \times 100 \quad (1)$$

where A₀ is the initial concentration of MB and A_i is the concentration of MB at pre-determined time intervals.

2.7 Hydroxyl radical measurement

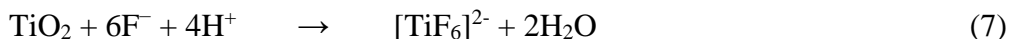
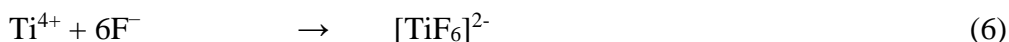
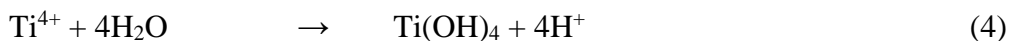
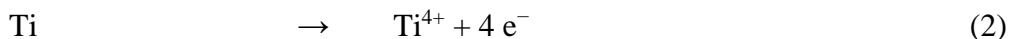
The amount of hydroxyl radical of the as-prepared TiO₂ nanotubes films was evaluated by using terephthalic acid as •OH scavenger [31]. The experimental procedures were similar to a previous study

[32] by measuring the emission peak at 425 nm (excitation wavelength 315 nm) using fluorescence analysis (Perkin Elmer LS-50B Luminescence Spectrometer).

3. RESULTS AND DISCUSSION

3.1 Microstructure and optical property

Normally, the formation of TNT in the anodization process depends on three simultaneous reactions: field-assisted oxidation of Ti metal to form TiO_2 , field-assisted etching of the oxide layer by the electric field weakening the bond between Ti and O, and the chemical dissolution of TiO_2 by fluoride ions [33-35]. The growth of TNT is a result of competition between electrochemical oxide formation (Eqs. (2)–(5)) and chemical dissolution of the oxide by F^- ions producing $[\text{TiF}_6]^{2-}$ complex ions (Eqs. (6) and (7)) by fluoride ions [36-38]. Initially, the oxide growth at the surface of the metal occurs due to interaction of the metal with O_2^- or OH^- ions. Then, these anions migrate through the oxide layer reaching the metal–oxide interface where they react with the metal. The defects on the surface of titanium results in induced field-assisted dissolution of the oxide layer. Thus a certain degree of solubility of the oxide in the electrolyte is needed to provide continuous oxide growth for the building up of nanotubular structures. During the anodization process, hydrogen forms at the counter electrode (platinum electrode) at the same time (Eq.8). The TiO_2 nanotube growth via the anodization process involves the following equations;



A typical current-time curve of TNT formation during anodization process is shown in Figure 2. At the first stage (stage I), the current quickly decreases to a minimum value due to the formation of a dense oxide layer. In the second stage (stage II), the current subsequently rises to a maximum, the pore nucleation phase occurs on the surface. These pores start to grow the tubular structure TiO_2 . For stage III, the current becomes constant, continuous growth of the tubes can be achieved. Moreover, the color change at surface of anode is observed due to the thickness of TiO_2 layer increases during anodization.

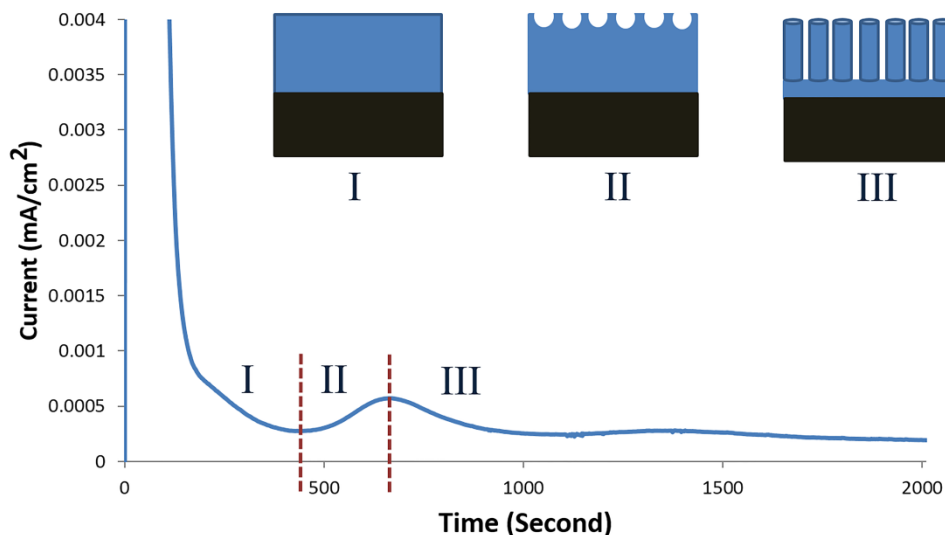


Figure 2. Current-time transient for TNT sample anodized under 0.8wt% NH_4F mixed with 2wt% H_2O in ethylene glycol electrolyte with 60 V for 35 min. Inset: illustration of the tubular nanostructure of the TiO_2 film.

To find the optimized anodization parameters, the effect of NH_4F concentrations on nanotube growth in the ethylene glycol electrolyte system was investigated. Figure 3 shows the morphologies of the TiO_2 films. The TNT was obtained at a higher NH_4F concentration, while the ordered tubular structure was not observed at a lower NH_4F concentration. These results clearly indicate that under suitable fluoride content, the self-organization can take place. At higher fluoride concentrations, TiO_2 nanotube arrays can hardly be obtained, because the released Ti^{4+} will react with F^- immediately and form soluble TiF_6^{2-} species. At lower concentrations of fluoride, an inefficient tube growth was obtained [33, 39]. The appearance of a well-organized TiO_2 nanotube array was illustrated in Figure 4, with a nanotube diameter of 85 nm and length of about 625 nm. The obtained well-organized TiO_2 nanotube array condition is used to modify the surface with curcumin.

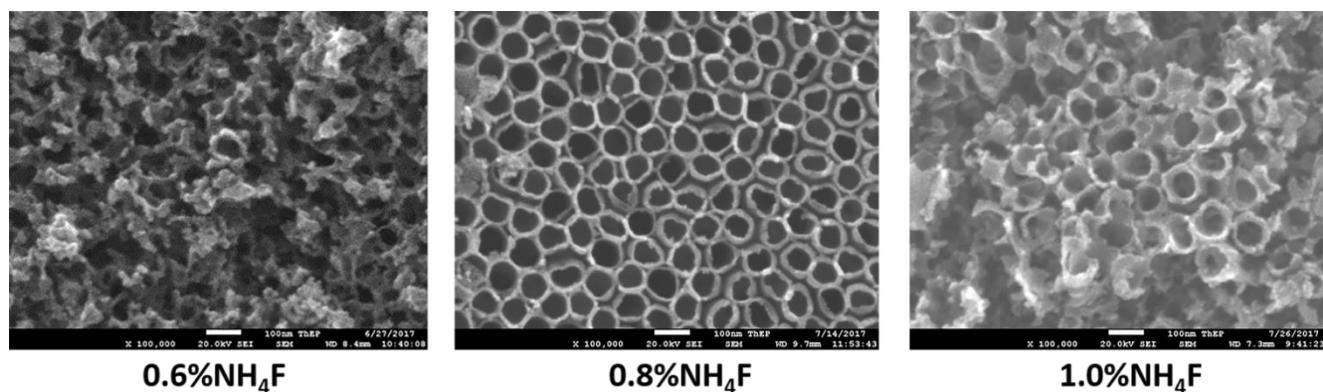


Figure 3. FE-SEM images of the obtained TiO_2 films at different concentrations of NH_4F mixed with 2wt% H_2O in ethylene glycol electrolyte under 60 V 35 min.

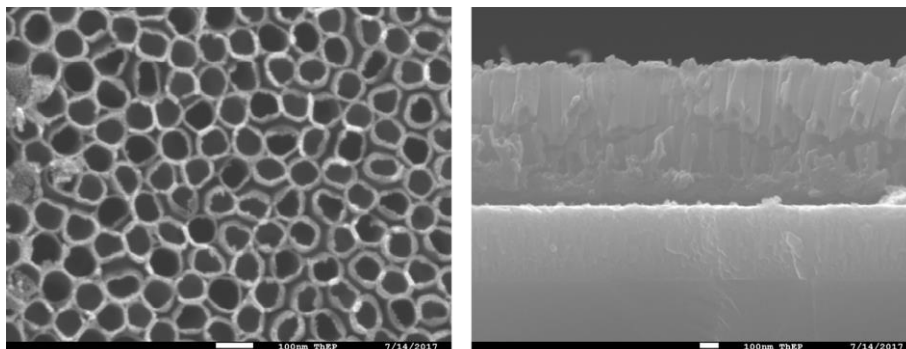


Figure 4. FE-SEM images of the optimized TNT prepared in ethylene glycol electrolyte containing 0.8 wt% NH_4F mixed with 2wt% H_2O under 60 V for 35 min.

The morphologies of the as-prepared TiO_2 nanotubes films were evaluated by SEM technique as illustrated in Figure 5. As shown in the figure, regular and highly ordered nanotube arrays surface was obtained using the anodization method. The diameters of pure TNT film and Cur-TNT films were approximately 85 nm. Comparison of these pure TNT films and Cur-TNT films revealed some defects in the Cur-TNT films possibly due to curcumin agglomeration on the surface of TiO_2 nanotubes. EDS was used to study the composition in the products (Figure 6) which showed the existence of Ti, O, C in the Cur-TNT films. This EDS analysis confirmed the presence of curcumin on the surface of TiO_2 .

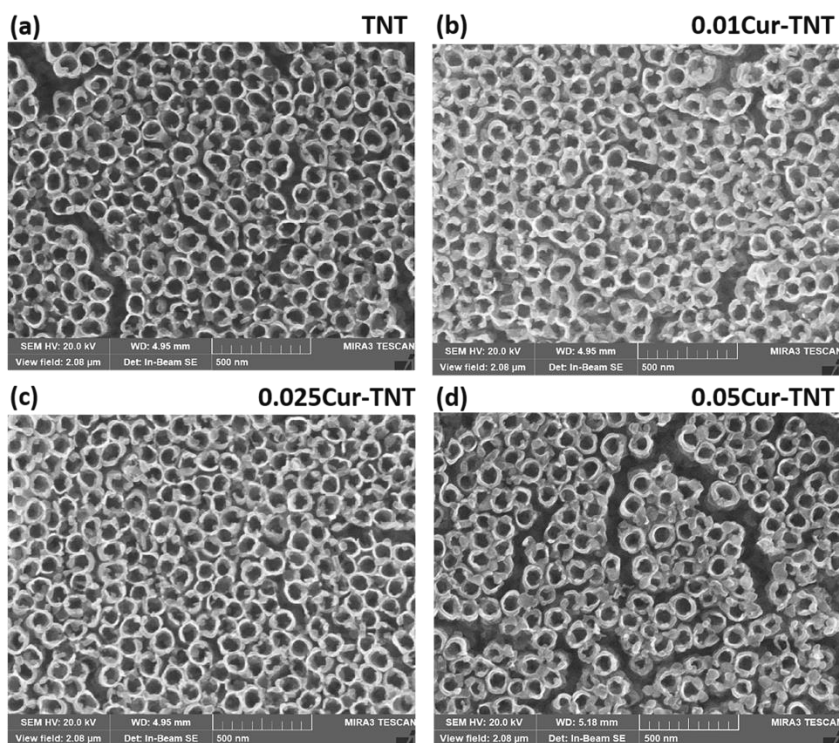


Figure 5. SEM images of (a) TNT (b) 0.01Cur-TNT (c) 0.025Cur-TNT and (d) 0.05Cur-TNT samples prepared in ethylene glycol electrolyte containing 0.8wt% NH_4F mixed with 2wt% H_2O under 60 V for 35 min.

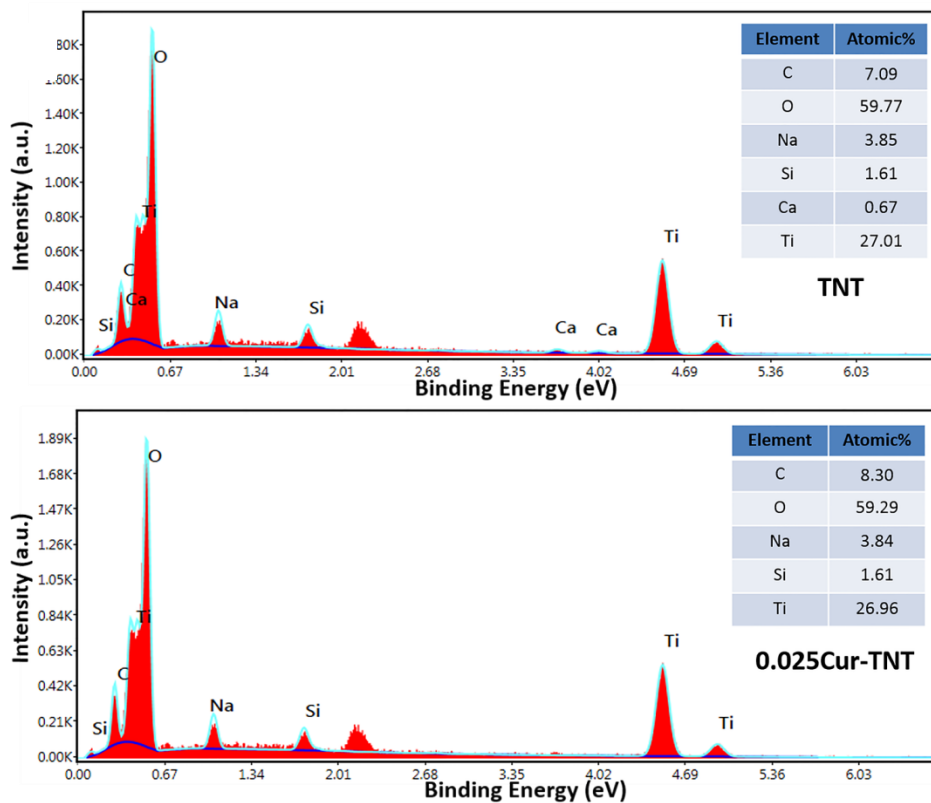


Figure 6. EDS spectra and Mapping analysis of TNT and Cur-TNT films.

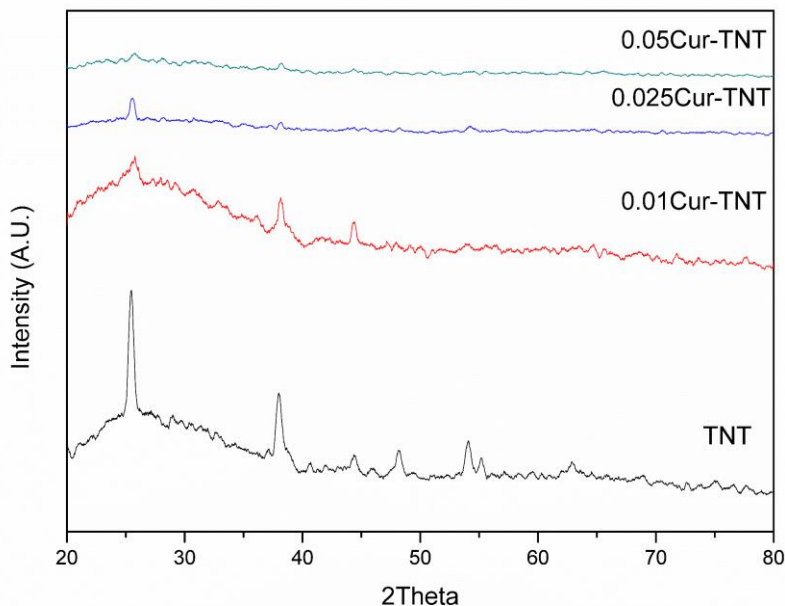


Figure 7. XRD patterns of TNT on glass and Cur-TNT films.

The XRD diffraction patterns of the TNT and Cur-TNT films are shown in Figure 7. It can be seen that all diffraction peaks of TNT and Cur-TNT films corresponded to the anatase phase (JCPDS 21-1272) [6]. The predominant anatase face of (101), (004) and other faces were detected. For Cur-TNT

films, it was revealed that the intensity of the anatase peak decreased possibly due to the high amount of curcumin on the surface of the TiO₂ film, consistent with the EDS results.

The surface chemical composition was investigated with Fourier-transformed infrared spectroscopy (FT-IR) as shown in Figure 8. Both TNT and Cur-TNT films revealed vibration bands of the Ti-O bond (400-800 cm⁻¹) [6] and the surface adsorbed H₂O (3000-3600 cm⁻¹) [6] and at 1640 cm⁻¹ [6]. The Cur-TNT films exhibited characteristic bands of TiO₂ (Ti-O band and -OH group) and curcumin (-CH₂, -CH₃ and C-O, C=O, C-C, C=C bond [40]) indicating its presence on the surface of these Cur-TNT films.

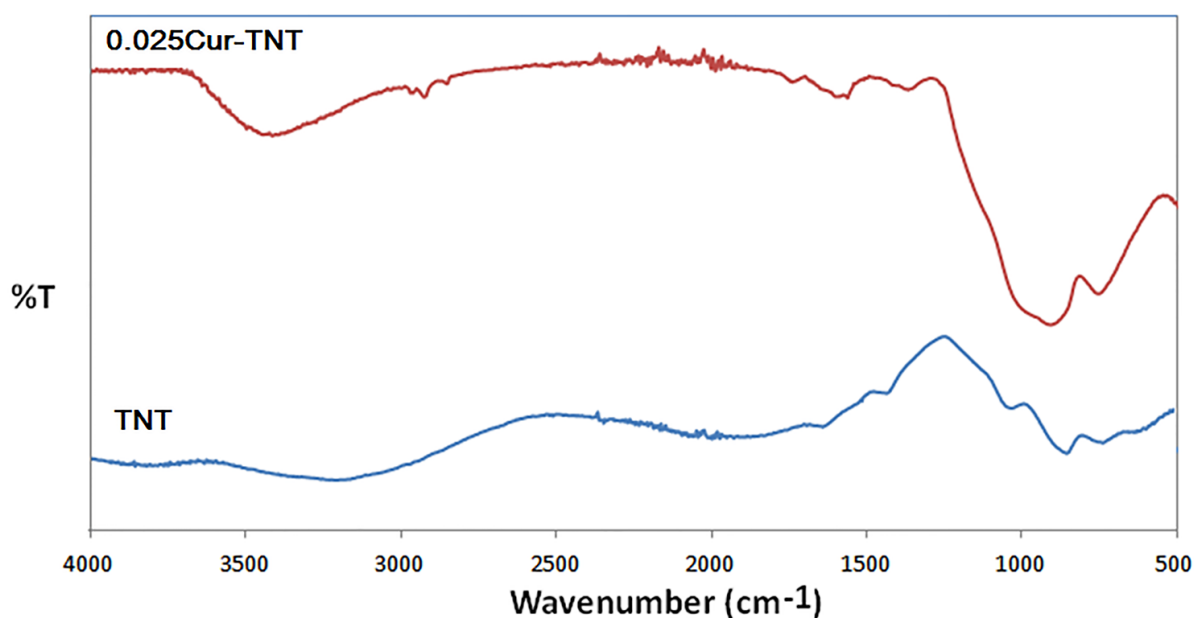


Figure 8. FT-IR spectra of TNT and Cur-TNT samples.

The optical properties and band gap energy of the TNT and Cur-TNT films were measured using diffused reflectance UV-Vis spectroscopy (DRS) as shown in Figure 9. DRS results showed that the Cur-TNT films exhibited more extended photoabsorption into the visible light region than the pure TNT films. The red shift of the Cur-TNT spectra should enhance photocatalytic efficiency under visible light. The band gap energies of the Cur-TNT films were calculated using equation (9):

$$E_g = \frac{hc}{\lambda} = \frac{1240}{\lambda} \quad (9)$$

where E_g is the band gap energy (eV); h is the Planck's constant (6.626×10^{-34} Js); c is the light velocity (3×10^8 m/s) and λ is the wavelength (nm). The calculated band gap energy of the curcumin modified TNT films decreased when compared with pure TNT films as shown in Table 1.

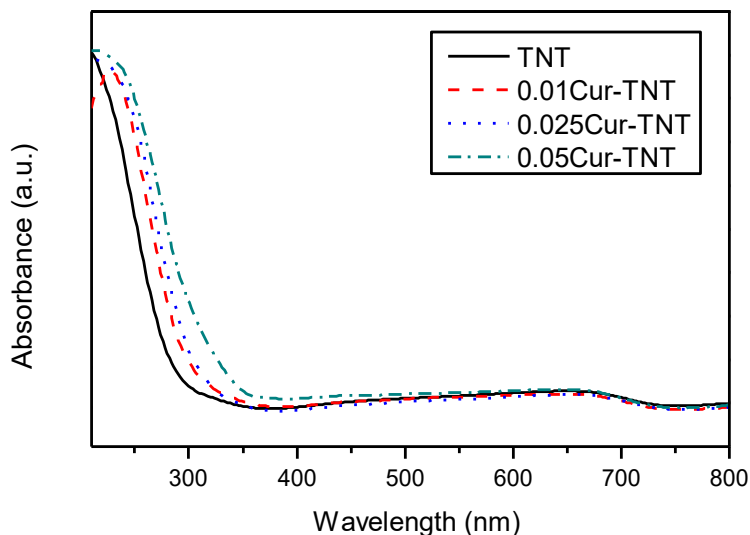


Figure 9. The absorption spectra of the TNT and Cur-TNT samples.

Table 1. Calculated band gap energy of the prepared TNT and Cur-TNT samples

TiO ₂ photocatalysts	Band gap energy (eV)
TNT	3.76
0.01Cur-TNT	3.70
0.025Cur-TNT	3.65
0.05Cur-TNT	3.10

3.2 Photocatalytic activity

The photocatalytic degradation of methylene blue using the TNT and the Cur-TNT films was examined under visible light irradiation. The photocatalytic results as shown in Figure 10 revealed that the Cur-TNT films exhibited higher photocatalytic activity than unmodified TNT films. The Cur-TNT films can generate more hydroxyl radicals than unmodified TNT films due to the good optical absorption in the visible region with more hydroxyl group adsorbed on the catalyst surface giving rise to a higher photocatalytic performance as shown in Figure 11. At higher curcumin loading, the agglomerated curcumin could become a recombination center of electron-holes resulting in a high recombination rate and hence a lower degradation efficiency.

The photocatalytic dye degradation exhibited by the Cur-TNT film under visible light irradiation may be explained as shown in Figure 12. When illuminated with visible light, curcumin sensitization can be achieved as the curcumin molecules (Eq. (10)) adsorbed on the surface of TiO₂ can be excited by $h\nu$, then the photo-induced electrons were injected into the conduction band of TiO₂ (Eq. (11)).

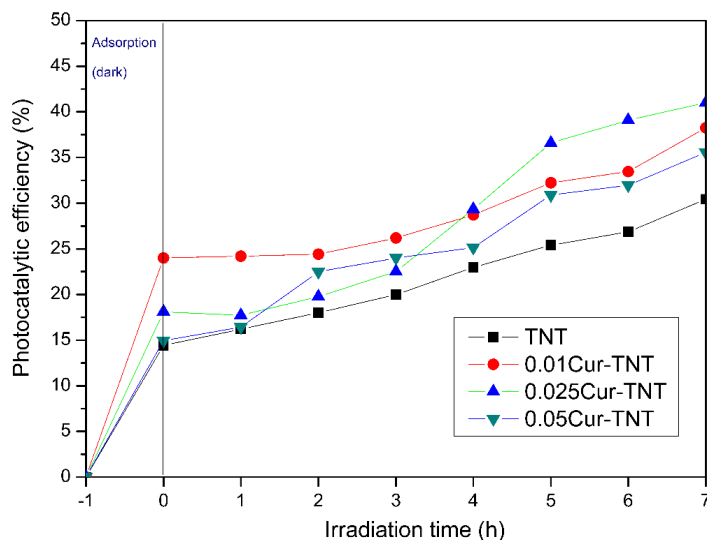


Figure 10. Comparison of the photodegradation efficiencies of methylene blue using the TNT and the Cur-TNT samples under visible light irradiation.

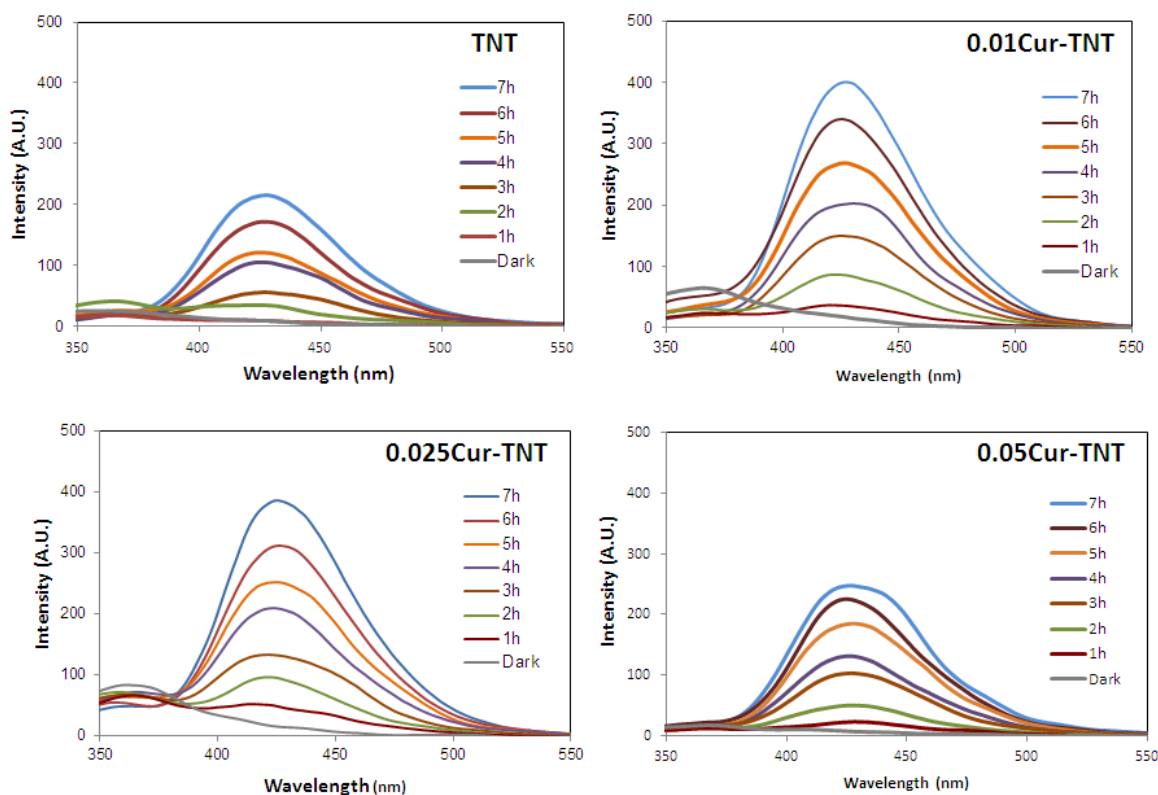


Figure 11. Comparison of the amount of $\bullet\text{OH}$ radical produced during the photocatalytic process using the TNT and the Cur-TNT samples under visible light irradiation.

Subsequently, the reactive electrons ($e_{cb}^{\bullet-}$ (TiO_2)) in the conduction band can reduce the O_2 adsorbed on the surface of TiO_2 to become the superoxide anion $\text{O}_2^{\bullet-}$, which can be further transformed into H_2O_2 and $\bullet\text{OH}$, resulting in the oxidation of MB (12)–(16). The pollutant molecules are attacked by the very reactive $\bullet\text{OH}$ and destroyed. Meanwhile, the reactive holes (h^+) can oxidize MB to its radical cation either directly or through a primarily formed $\bullet\text{OH}$ [41-43].

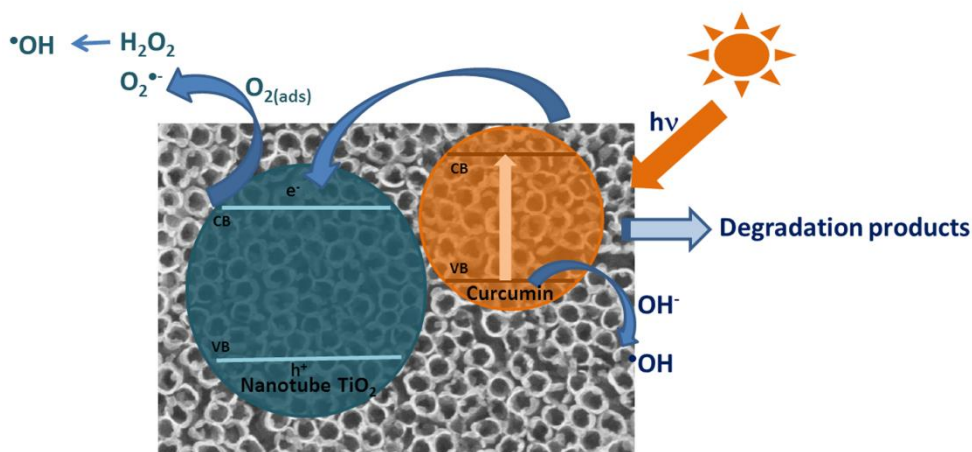
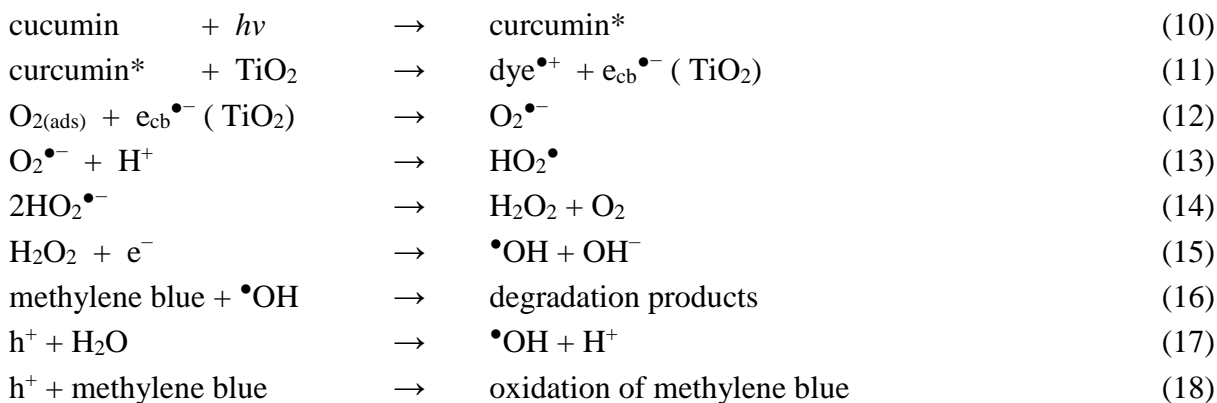


Figure 12. Schematic representation for photocatalytic activity of the Cur-TNT under visible light irradiation.

4. CONCLUSIONS

Curcumin modified nanotube TiO₂ films (Cur-TNT) were successfully prepared by a modified impregnation method. Different concentrations of curcumin content were studied. The physical properties of the Cur-TNT films were studied by several techniques such as XRD, SEM, FT-IR, and DRS. The TiO₂ phase in both TNT and Cur-TNT samples were anatase. SEM images revealed that the synthesized TiO₂ films have nanotube-like structures. The DRS results revealed that the Cur-TNT samples showed extended absorbance into the visible region. The photocatalytic performances of the Cur-TNT samples exhibited higher photocatalytic performance than the pure TNT samples under visible light irradiation since the 0.025Cur-TNT sample produced a higher concentration of hydroxyl radicals than the pure TNT sample under visible light irradiation. Moreover, the curcumin dopant also played the role of inducing light absorption in the visible region to generate more e⁻-h⁺ pairs, resulting in improvement of the photocatalytic activity and stability.

ACKNOWLEDGMENTS

The author would like to thank the Faculty of Science, Silpakorn University, Nakornpathom, Thailand for financial support (Grant No. SRF-JRG-2560-11).

References

1. A. Fujishima, K. Honda, *Nature*, 238 (1972) 37.
2. M. R. Hoffmann, S. T. Martin, W. Choi, D. W. Bahnemann., *Chem.Rev.*, 95 (1995) 69.
3. P. V. Kamat, *Chem. Rev.*, 93 (1993) 267.
4. Y. Zheng, C. Chen, Y. Zhan, X. Lin, Q. Zheng, K. Wei, J. Zhu, *J. Phys. Chem. C*, 112 (2008) 10773.
5. D. Chen, Y. Li, J. Zhang, J. Z. Zhou, Y. Guo, H. Liu, *Chem. Eng. J.*, 185–186 (2012) 120.
6. C. Suwanchawalit, S. Wongnawa, P. Sriprang, P. Meanha, *Ceram. Int.*, 38 (2012) 5201.
7. H. Y. Chuang, D. H. Chen, *Nanotechnology*, 20 (2009) 105704.
8. H. Moradi, A. Eshaghi, S. R. Hosseini, K. Ghani, *Ultrason. Sonochem.*, 32 (2016) 314.
9. C. Liu, J. Wang, W. Chen, C. Dong, C. Li, *Chem. Eng. J.*, 280 (2015) 588.
10. Q. Wang, Z. Qin, J. Chen, B. Ren, Q. Chen, Y. Guo, X. Cao, *Appl. Surf. Sci.*, 364 (2016) 1.
11. S. Buddee, S. Wongnawa, U. Sirimahachai, W. Puetpaibool, *Mater. Chem. Phys.*, 126 (2011) 167.
12. J. Liu, L. Han, N. An, L. Xing, H. Ma, L. Cheng, J. Yang, Q. Zhang, *Appl. Catal. B: Environ.*, 202 (2017) 642.
13. Y. Cong, J. Zhang, F. Chen, M. Anpo, *J. Phys. Chem. C*, 111 (2007) 6976.
14. X. Chen, D. H. Kuo, D. Lu, *Adv. Powder Technol.*, 28 (2017) 1213.
15. W. Yu, X. Liu, L. Pan, J. Li, J. Liu, J. Zhang, P. Li, C. Chen, Z. Sun, *Appl. Surf. Sci.*, 319 (2014) 107.
16. C. Wang, J. Li, G. Mele, G. M. Yang, F. X. Zhang, L. Palmisano, G. Vasapollo, *Appl. Catal. B: Environ.*, 76 (2007) 218.
17. T. V. Nguyen, J. C. S. Wu, C. H. Chiou, *Catal. Commun.*, 9 (2008) 2073.
18. M. K. Nazeeruddin, R. Humphry-Baker, M. Gratzel, D. Wöhrle, G. Schnurpfeil, G. Schneider, A. Hirth, N. Trombach, *J. Porphyrins Phthalocyanines*, 3 (1999) 230.
19. X. Shang, B. Li, C. Li, X. Wang, T. Zhang, S. Jiang, *Dyes Pigm.*, 98 (2013) 358.
20. A. Martinez-de la Cruz, U. M. Garcia Perez, *Mater. Res. Bull.*, 45 (2010) 135.
21. L. Huang, F. Peng, H. Wang, H. Yu, Z. Li, *Catal. Commun.*, 10 (2009) 1839.
22. L. Tan, X. Zhang, Q. Liu, X. Jing, J. Liu, D. Song, S. Hu, L. Liu, J. Wang, *Colloids Surf. A*, 469 (2015) 279.
23. S. Ananth, T. Arumanayagam, P. Vivek, P. Murugakoothan, *Optik*, 125 (2014) 495.
24. K. S. Raja, Y. R. Smith, N. Kondamudi, A. Manivannan, M. Misra, V. R. Subramanian, *Electrochem. Solid-State Lett.*, 14 (2011) F5.
25. W. Jiang, Y. Ling, S. Hao, H. Li, X. Bai, D. Cang, *Key Eng. Mater.*, 336-338 (2007) 2200.
26. S. Kathirvel, C. Su, C. -Y. Yang, Y. -J. Shiao, B. -R. Chen, W. -R. Li, *Vacuum*, 118 (2015) 17.
27. B. -G. Lee, J. -W. Choi, S. -E. Lee, Y. -S. Jeong, H. -J. Oh, C. -S. Chi, *Trans. Nonferrous Met. Soc. China.*, 19 (2009) 842.
28. Y. R. Smith, R. S. Ray, K. Carlson, B. Sarma, M. Misra, *Materials*, 6 (2013) 2892.
29. C. Suwanchawalit, V. Somjit, *Dig. J. Nanomater. Biostruct.*, 10 (2015) 705.
30. C. Suwanchawalit, V. Somjit, *Dig. J. Nanomater. Biostruct.*, 10 (2015) 769.
31. O. Mehraj, N.A. Mir, B.M. Pirzada, S. Sabir, M. Muneer, *J. Mol. Catal. A: Chem.*, 395 (2014) 16.
32. S. Buddee, C. Suwanchawalit, S. Wongnawa, *Dig. J. Nanomater. Biostruct.*, 12 (2017) 829.
33. Q. H. Chen, H. L. Liu, Y. J. Xin, X. W. Cheng, J. Zhang, J. J. Li, P. Wang, H. J. Li, *Electrochim. Acta*, 99 (2013) 152.
34. A. Haring, A. Morris, M. Hu, *Materials*, 5 (2012) 1890.
35. P. Roy, S. Berger, P. Schmuki, *Angew. Chem. Int. Ed.*, 50 (2011) 2904.

36. K. Yasuda, J. M. Macak, S. Berger, A. Ghicov, P. Schmuki, *J. Electrochem. Soc.*, 154 (2007) C472.
37. R. X. Ge, W. Y. Fu, H. B. Yang, Y. Y. Zhang, W. Y. Zhao, Z. L. Liu, C. J. Wang, H. Y. Zhu, Q. J. Yu, G. T. Zou, *Mater. Lett.*, 62 (2008) 2688.
38. C.B. Marien, T. Cottinea, D. Robert, P. Drogui, *Appl. Catal. B: Environ*, 194 (2016) 1.
39. Z. B. Xie, D. J. Blackwood, *Electrochim. Acta*, 56 (2010) 905.
40. S. Buddee, S. Wongnawa, P. Sriprang, C. Sriwong, *J. Nanopart. Res.*, 16 (2014) 2336.
41. P. -C. Yao, S. -T. Hang, C. -W. Lin, D. -H. Hai, *J. Taiwan Inst. Chem. Eng.*, 42 (2011) 470.
42. A. Kathiravan, R. Renganathan, *J. Colloid Interface Sci.*, 331 (2009) 401.
43. D. Chen, D. Yang, J. Geng, J. Zhu, Z. Jiang, *App. Surf. Sci.*, 255 (2008) 2879.

© 2019 The Authors. Published by ESG (www.electrochemsci.org). This article is an open access article distributed under the terms and conditions of the Creative Commons Attribution license (<http://creativecommons.org/licenses/by/4.0/>).